Performance Analysis of Rare-earth and Rare-earth free External Rotor Motors under Eccentricity Faults

Sai Sudheer Reddy Bonthu, *IEEE Member,* Md. Tawhid Bin Tarek, *IEEE Student Member,* Md. Zakirul Islam, *IEEE Student Member,* and Seungdeog Choi, *IEEE Senior Member*

Department of Electrical and Computer Engineering
The University of Akron, USA
sb158@zips.uakron.edu, schoi@uakron.edu

***Abstract*— This paper presents the performance comparisons between rare-earth and rare-earth free external rotor permanent magnet assisted synchronous reluctance motors (PMa-SynRMs) under static eccentricity (SE), dynamic eccentricity (DE), and mixed eccentricity (ME) conditions. Recently, external rotor motors are proposed as high power density motors for traction applications in electric vehicles and more electric aircraft. However, these in-wheel external rotor motors are usually under continuous stress of rotational forces due to the tire-road friction which can result in eccentricity faults due to stator and rotor misalignment. Therefore, it is critical to assess the external rotor motors performance under eccentricity faults in traction motors. In this study, various failure modes due to eccentricity faults such as SE, DE, and ME conditions are analyzed on optimal 3.8kW rare-earth based and 3.7kW rare-earth free external rotor PMa-SynRMs. Effects of these eccentricity conditions are translated to performance loss in terms of increased torque ripple and unbalanced magnetic pull (UMP) in the electric motor designs. Also, 3rd harmonics of back-electromotive force (back-EMF) have been analyzed for both motors in all eccentricity conditions to compare their performance in fault detection. Experimental setup is developed to test the motors under load conditions and finite element simulation results are presented to validate the proposed theory.**

***Keywords*— eccentricity, permanent magnet (PM) motors, reluctance machines, multi-phase machines, finite element method, electromagnetic forces**

Nomenclature

F_r	UMP on the rotor
B_g	air-gap flux density
θ_r	rotor position with respect to the reference axis
φ_s	angle of any point on the stator inner surface from the reference axis
ω_m	rotor angular speed
$g^{-1}(\varphi_s)$	inverse air-gap function
N_c	total number of coils per phase
L_{stk}	Stack length of the machine
k_{wh}	Winding function
μ_0	permeability of air
U_h	*h-th* harmonic component of the magnetic potential difference in the air-gap
E_{jh}	magnitude of the h-th harmonic of *j-th* phase's back-emf
N_i	number of conductors in the *i-th* coil
α_i	angle of first coil side of *i-th* coil
D	Rotor bore diameter

I. INTRODUCTION

Eccentricity faults occur due to manufacturing intolerances which result in stator and rotor misalignment from the center-axis of rotation. In last two decades, eccentricity faults and their effects on the electric motor performance have been investigated in detail [1, 2]. Eccentricity faults can be categorized as static-eccentricity (SE), dynamic eccentricity (DE), and mixed-eccentricity (ME). Due to eccentricity faults, the motor performance is degraded. Several research methodologies have been proposed depict the performance degradation due to the eccentricity type and the degree of eccentricity in traction motor applications [3-5]. External rotor motors which are proposed for high power density applications such as more electric aircraft, are highly prone to eccentricity faults due to their in-wheel capability and space constraint [7]. However, there has been limited study on eccentricity analysis on traditional outer rotor BLDC motors to the best of author's knowledge. Hence, the external rotor motors need to be investigated under eccentricity faults.

In addition to the outer rotor capability, the in-wheel rotor motors develop higher torque at higher speeds [8] compared to the internal rotor motor designs which results

in higher stress on the outer rotor which might result in unbalance magnetic pull (UMP) in addition to the manufacturing intolerances such as eccentricity conditions.

In this study, two high torque density five-phase external rotor motor configurations [9] with rare-earth material neodymium (Nd) magnets and rare-earth free material ferrite (Fe) magnets are utilized to compare their performances under various eccentricity faults. The design of the external rotor permanent magnet assisted synchronous reluctance motors (PMa-SynRMs) [10] is discussed in detail. Numerical analysis to depict the UMP resulted due to eccentricity is presented. Performance degradation in terms of decrease in average torque developed and increase in torque pulsations is considered as the comparison index between rare-earth and rare-earth free PMa-SynRMs. Furthermore, to validate the simulations, 3.8kW dynamo setup with five-phase inverter and prototypes are developed.

II. Eccentricity Faults in External Rotor Motors

This section discusses the optimal selection of pole/slot combination, flux barrier design and demagnetization characteristics for the proposed five-phase PMa-SynRM designs. Table I summarizes the design specifications of the external rotor PMa-SynRMs. External rotor motors that are optimally designed [9-12] for high torque density and low torque ripple traction applications are utilized to conduct eccentricity fault analysis. Finally, results are tabulated and deductions are plotted.

TABLE I
DESIGN SPECIFICATIONS

Design parameter	Value
number of poles, *p*	12
number of slots	25
slots/pole/phase (SPP) ratio	0.42
stator back iron depth (mm)	20
total stator slot area (mm^2)	7964.4
rotor cross-section area (mm^2)	5988.73
number of turns/coil	25
rotor/stator outer diameter (mm)	190

TABLE II
RATED TORQUE & TORQUE RIPPLE OF EXTERNAL MOTORS

Motor Type	Average Torque (N-m)	Torque Ripple(%)
Rare-earth	19.68	4.90
Rare-earth free	19.20	4.80

Five-phase 3.8kW rare-earth PM based and 3.7kW ferrite PM based PMa-SynRMs with same rotor outer diameters of 190mm are utilized in this study to conduct eccentricity fault analysis. Fig. 1 (a) and (b) depict the cross sections of the external rotor finite element models. Table II summarizes the average torque developed and torque pulsations at rated current and speed for rare-earth and rare-earth free external rotor PMa-SynRMs, respectively.

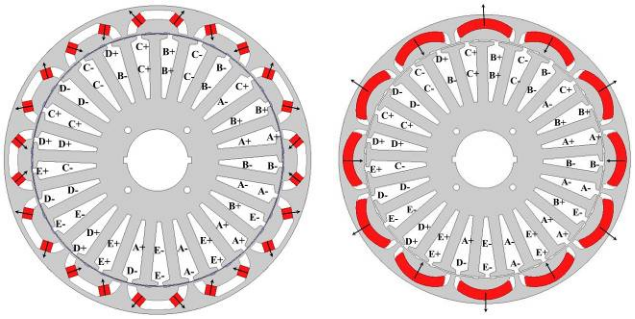

(a) (b)

Fig. 1. Five-phase external rotor PMa-SynRM FEA designs with magnetization directions: (a) rare-earth (Nd) and (b) ferrite based PMs.

III. Simulation Results under Eccentricity Faults

Under SE, DE, and ME eccentricity conditions, simulations are carried out to depict the results for the average torque developed and torque developed. Due to space constraint, ME results will be included in full paper.

A. Static Eccentricity

Static-Eccentricity (SE) is the most common failure of the three eccentric faults in electric motors. SE occurs in electric motors when the rotor along with the center-axis of rotation moves away from the stator center as shown in Fig. 2 (a). Simulation results are presented in Fig. 2 (b) and (c). Table III summarizes the torque ripple results at different degrees of SE. For the rare-earth motor, average torque increased by 0.91% from healthy to 40% eccentricity condition. But at the same time, torque ripple increased by 4.55% when the degree of eccentricity reaches 40%.

For rare-earth free motor, average torque decreased by 0.58% for 40% eccentricity condition. In this case, the increase in torque ripple is 6.26%, which is higher than that of rare-earth motor.

B. Dynamic Eccentricity

In DE, as shown in Fig. 3 (a), the rotation axis of rotor shifts away from the stator and motor center of rotation. Based on the stator and center-axis of rotation shift from the center of the rotor, various degrees of DE faults are created in the simulation model and results are presented in Fig. 3 (b). Table IV summarizes the torque ripple results at different degrees of DE. Average torque decreased by 3.62% for rare-earth motor when the degree of eccentricity changes from 0 to 40%. Here, torque ripple also increased by 8.3%.

For rare-earth free motor, the decrease in average torque is 1.71% which is relatively smaller than that of rare-earth motor. However, torque ripple increases by 9.13%, which is higher than that of rare-earth motor.

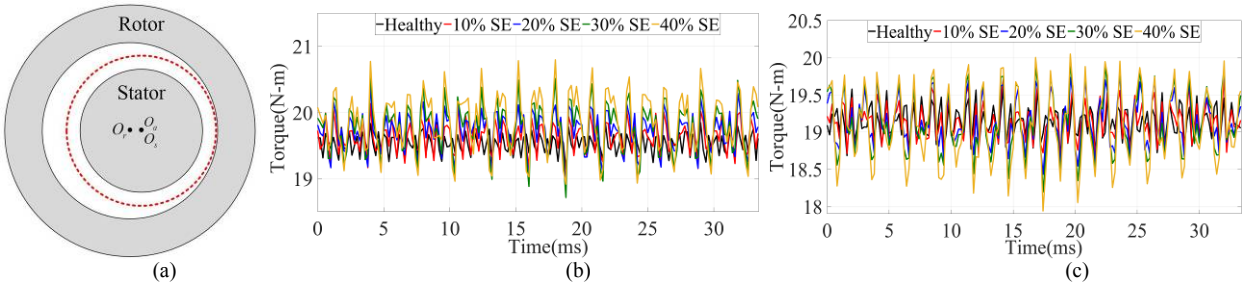

(a) (b) (c)

Fig. 2. External rotor motor: (a) SE fault, (b) rare-earth design with 10%-40% SE faults, and (c) rare-earth free design with 10%-40% SE faults

TABLE III
STATIC-ECCENTRICITY

Static-Eccentricity	*Rare-earth design*		*Rare-earth free design*	
	Avg. Torque (Nm)	*Torque Ripple (%)*	*Avg. Torque (Nm)*	*Torque Ripple (%)*
10% - S_1	19.617	6.17	19.144	5.95
20% - S_2	19.709	8.57	19.151	7.34
30% - S_3	19.776	9.59	19.126	9.13
40% - S_4	19.859	9.45	19.088	11.06

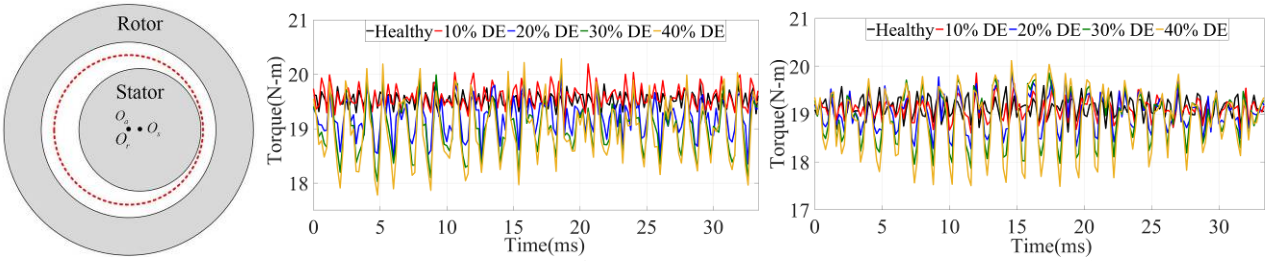

(a) (b) (c)

Fig. 3. External rotor motor: (a) DE fault, (b) rare-earth design with 10%-40% DE faults, and (c) rare-earth free design with 10%-40% DE faults

TABLE IV
DYNAMIC-ECCENTRICITY

Dynamic-eccentricity	*Rare-earth design*		*Rare-earth free design*	
	Avg. Torque (Nm)	*Torque Ripple (%)*	*Avg. Torque (Nm)*	*Torque Ripple (%)*
10% - D_1	19.591	6.09	19.130	6.56
20% - D_2	19.213	8.45	19.016	8.32
30% - D_3	19.043	11.32	18.946	11.29
40% - D_4	18.968	13.20	18.872	13.93

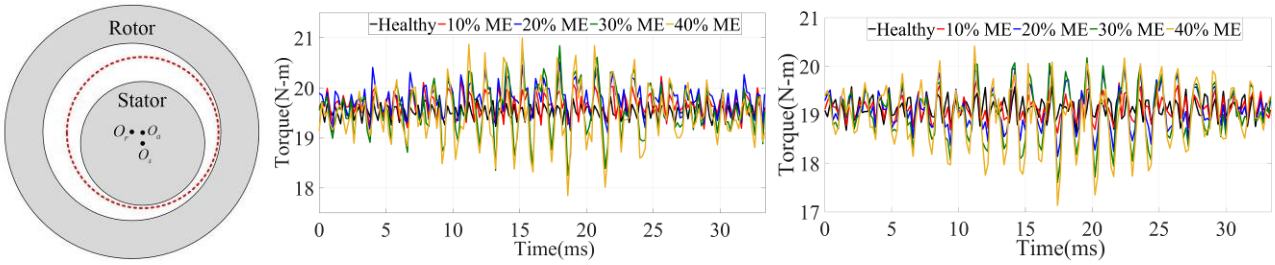

(a) (b) (c)

Fig. 4. External rotor motor: (a) ME fault, (b) rare-earth design with 10%-40% ME faults, and (c) rare-earth free design with 10%-40% ME faults

TABLE V
MIXED-ECCENTRICITY

Mixed-eccentricity	Rare-earth design		Rare-earth free design	
	Avg. Torque (Nm)	Torque Ripple (%)	Avg. Torque (Nm)	Torque Ripple (%)
10% - M1	19.591	6.09	19.130	6.56
20% - M2	19.213	8.45	19.016	8.32
30% - M3	19.043	11.32	18.946	11.29
40% - M4	18.968	13.20	18.872	13.93

C. *Mixed Eccentricity*

In ME, as shown in Fig. 4 (a), the rotation axis of rotor shifts away from the stator and motor center of rotation. Based on the stator and center-axis of rotation shift from the center of the rotor, various degrees of ME faults are created in the simulation model and results are presented in Fig. 4 (b). Table V summarizes the torque ripple results at different degrees of ME.

From healthy to 40% eccentricity condition, the reduction in average torque is 1.06% for rare-earth motor. Furthermore, torque ripple increases by 11.28% for the same condition. Percentage decrease of average torque for rare-earth free motor is 1.26%, which is relatively lower than that of rare-earth motor. But increase in torque ripple for rare-earth free motor is 12.52%.

D. *Performance Comparison among Different Eccentricity Conditions*

For the rare-earth and rare-earth free external rotor motor, the change of average torque and torque are different for SE, DE and ME. Fig. 5 shows the trend of average torque and torque ripple for rare-earth external rotor motor when all three eccentricities are changed from 0 to 40%.

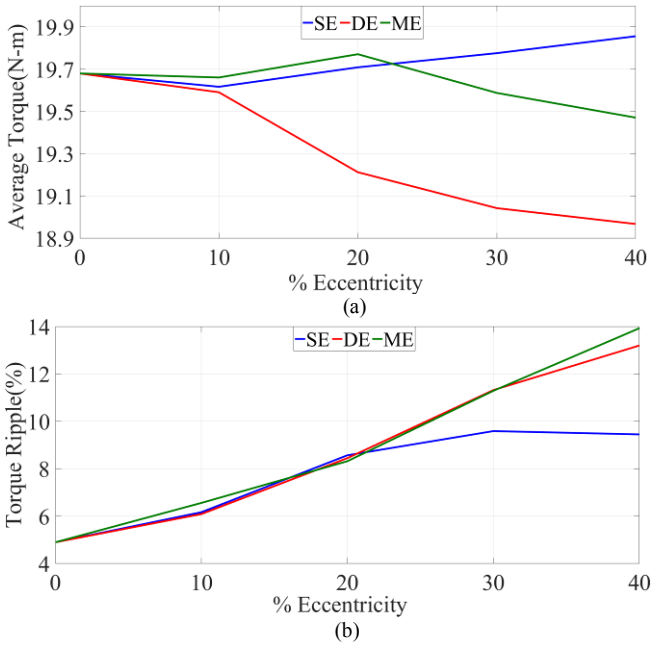

Fig. 5. (a) Average torque, (b) Torque ripple (%) trend for the rare-earth external rotor PMa-SynRM in all three eccentricity conditions.

For the rare-earth motor, DE has the highest impact on torque reduction among all three eccentricities when degree of eccentricity is increasing. For the increase of toque ripple, both DE and ME have high impact, whereas ME has slightly higher impact.

Same performance analysis has been conducted for the rare-earth free external rotor PMa-SynRM. Fig. 6 shows the trend of average torque and torque ripple for rare-earth free external rotor motor when all three eccentricities are changed from 0 to 40%.

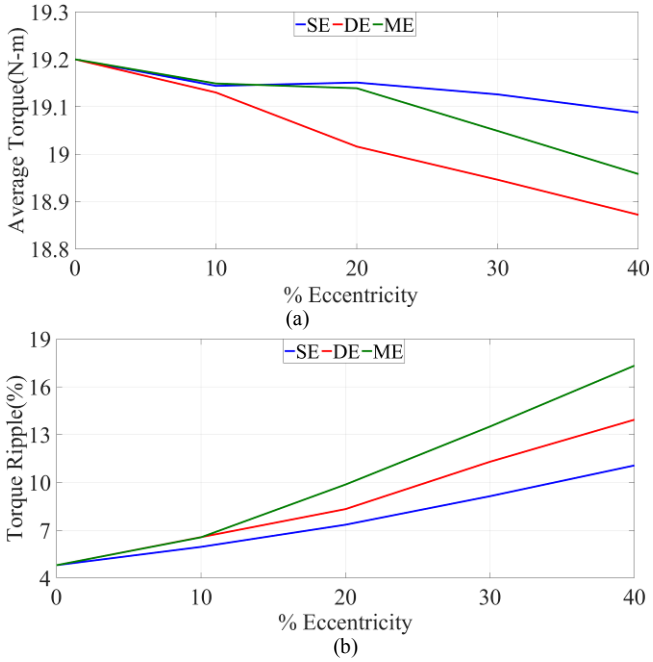

Fig. 6. (a) Average torque, (b) Torque ripple (%) trend for the rare-earth free external rotor PMa-SynRM in all three eccentricity conditions.

When the degree of eccentricity is increasing, DE has the highest impact on torque reduction among all three eccentricities. And for the torque ripple, if the degree of eccentricity is increasing, ME increases the ripple higher than those of other two eccentricities.

To summarize, for the both external rotor PMa-SynRMs, DE has the highest impact on torque reduction whereas ME has the highest impact on torque ripple increase.

IV. Unbalanced Magnetic Pull (UMP) on the Rotor

The rotor the discussed motors will experience UMP due to the existence of unbalanced magnetic flux distribution around the rotor. The eccentricity fault will increase the magnitude of UMP. The UMP on the rotor can be defined in terms of air-gap flux density as [13]:

$$F_r = \int_0^{2\pi} \frac{B_g^2(\theta_r)\,\mathrm{DL}_{\mathrm{stk}}}{4\mu_0} e^{j\theta_r} d\theta_r \qquad (1)$$

The eccentricity type and severity will determine the air-gap flux density which will affect the generated UMP according to (1).

Different levels and types of eccentricity have been incorporated in the FEA models of rare-earth based and rare-earth free external rotor PMa-SynRM models. Fig. 7

shows the maximum values of UMP on the rotor for zero to forty percent of SE and DE. The simulation result shows that rare-earth-free models will experience nearly 100 N higher UMP than rare-earth based models at any eccentricity level. This simulation results refer the air-gap flux density distribution in rare-earth-free external rotor PMa-SynRM model has higher unbalance than the rare-earth based model.

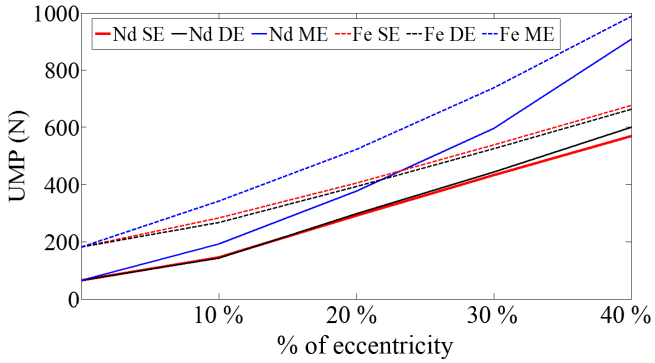

Fig. 7. Calculated UMP in rare-earth and rare-earth free external rotor PMa-SynRMs.

V. Comparisons of Back-EMF 3rd Harmonics in Fault Conditions

The eccentricity will generate harmonics in the air-gap density which will create additional harmonics components in the induced voltage. The back-emf of the j-th phase can be expressed for any healthy or eccentric PMa-SynRM as:

$$E_{jh} = \mu_0 w_m k_{wh} U_h \sum_{N_c} N_i \int_{\alpha_{ij}} g^{-1}(\varphi_s)\, \mathrm{d}\varphi_s \qquad (2)$$

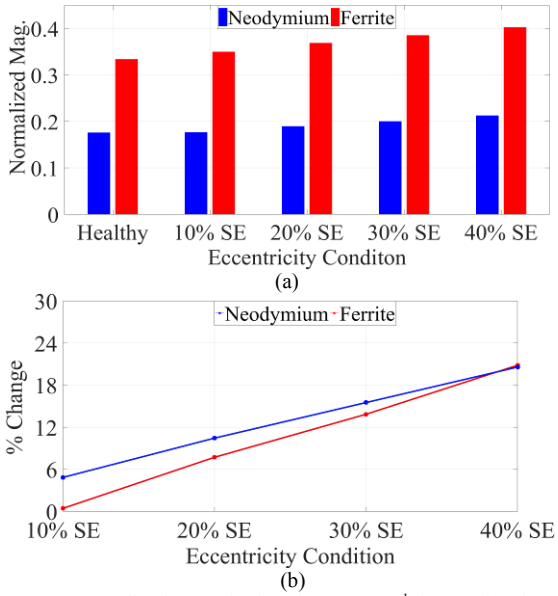

Fig. 8. (a) Normalized magnitude of BEMF 3rd harmonics in static-eccentricity conditions, (b) Percentage change in 3rd harmonics in compared to healthy condition.

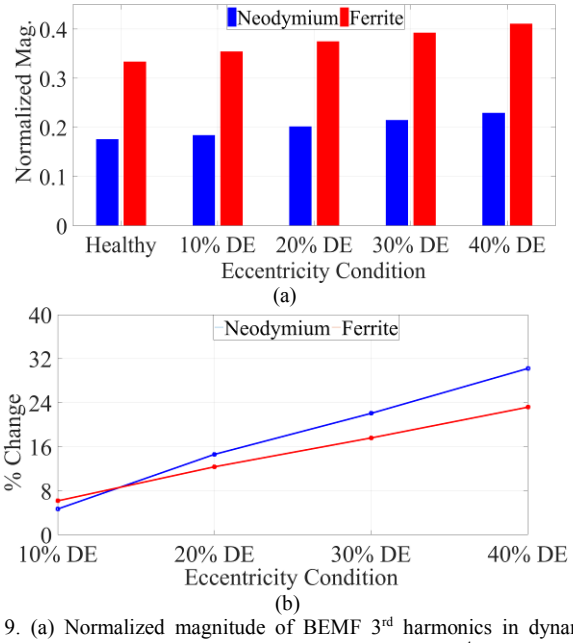

Fig. 9. (a) Normalized magnitude of BEMF 3rd harmonics in dynamic-eccentricity conditions, (b) Percentage change in 3rd harmonics in compared to healthy condition.

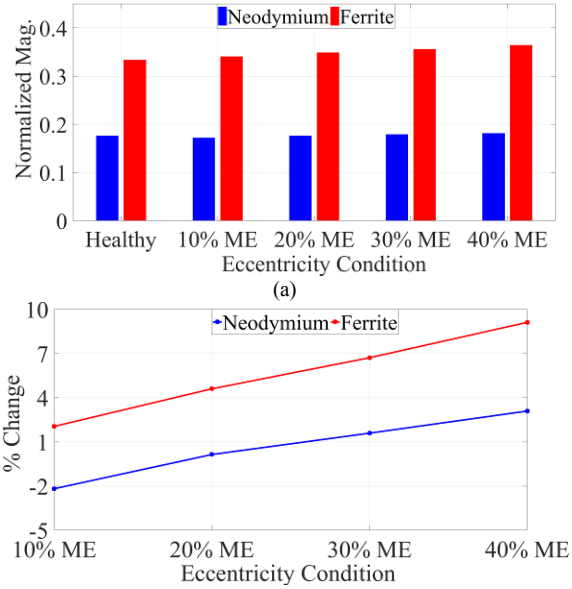

Fig. 10. (a) Normalized magnitude of BEMF 3rd harmonics in mixed-eccentricity conditions, (b) Percentage change in 3rd harmonics in compared to healthy condition.

The eccentricity type and severity will affect the inverse air-gap function which will modify the amplitudes of the back-EMF harmonics components. To understand the trend back-EMF harmonic contents of ferrite and neodymium based external rotor motor, fast Fourier transform (FFT) has been done for all three eccentricity conditions. Here, the main purpose is to analyze how the harmonic content varies in both motors for eccentricity conditions. To measure it, 3rd harmonics of back-EMF has been chosen as it is the most

dominant harmonics after fundamental. Fig. 8, Fig. 9, and Fig. 10 show the normalized 3rd harmonics percentage change in 3rd harmonics for static-, dynamic- and mixed-eccentricity conditions. As the air-gap flux density distribution in rare-earth-free external rotor PMa-SynRM model has higher unbalance than the rare-earth based model, the 3rd harmonics of back-EMF of rare-earth-free model is always higher than corresponding value of the rare-earth counterpart.

From Fig. 8, it is can be seen that, the normalized magnitude of back-EMF 3rd harmonics ferrite based external rotor motor is higher than neodymium based motor. For static eccentricity, percentage change in 3rd harmonics compared with healthy condition is higher for neodymium based motor. But with increasing degree of eccentricity, the difference deceases. In 40% static eccentricity, percentage change of neodymium motor surpasses the change of ferrite based motor. Figure 9 shows the normalized 3rd harmonics for both motors for dynamic eccentricity and percentage change in 3rd harmonics in these conditions. Percentage change of 3rd harmonics for ferrite based PMa-SynRM is higher in lower degree of dynamic eccentricity. As degree of dynamic eccentricity increases, percentage change in 3rd harmonics for neodymium motor surpasses ferrite based motor. This difference becomes higher with higher degree of dynamic eccentricity. Figure 10 summarizes normalized 3rd harmonics for rare-earth and rare-earth free under mixed eccentricity and percentage change in harmonics.

VI. Experimental Setup and Results

The optimal 3.7kW and 3.8kW five-phase external rotor PMa-SynRMs with 25 slots 12 poles are fabricated. Figure 11. (a) and (b) depict the rare-earth and rare-earth free external rotor PMa-SynRM prototypes. S18 steel has been utilized as the material for the stator and rotor cores. NdFe35 and Y32-H2 ferrite magnets are embedded in the rare-earth and rare-earth free rotor flux barrier designs respectively. A complete dynamo setup to test the fabricated prototype under no load conditions is presented in Fig. 11 (c).

No-load test results are included in this paper which present the phase to phase induced voltage in external rotor motors. Fig. 12 (a) and (b) [14, 15] depict the tested no-load back-EMF results for rare-earth and rare-earth free external rotor PMa-SynRMs at 1800rpm rated speed.

Although it is practically possible to test the eccentricity conditions by inducing intolerances into the bearing of electric motor designs, this study is limited to the proposal of impact due to different eccentricity conditions on in-wheel motors. Future publications will include detailed experimental analysis on eccentricity as the prototypes are under continuous testing phase at various speeds and torque levels.

(a) (b)

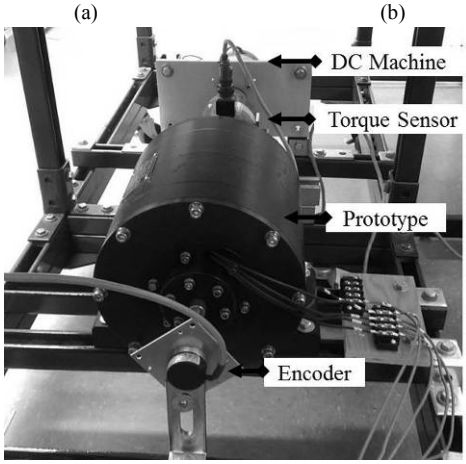

(c)

Fig. 11. Cross sections of fabricated 25 slot 12 pole five-phase external rotor PMa-SynRMs: (a) Nd PMs, (b) Fe PMs, and (c) dynamo setup.

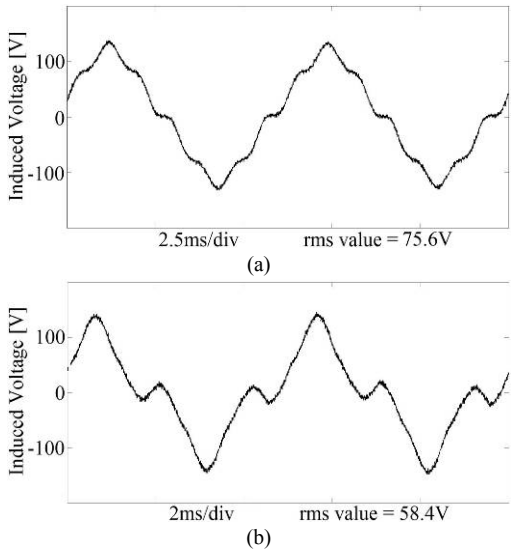

Fig. 12. No-load back-EMF results for (a) rare-earth and (b) rare-earth free PMa-SynRM.

VII. Conclusions

In this study, performances of five-phase external rotor PMa-SynRMs with SE, DE, and ME conditions are compared in detail. It has been observed that ferrite magnet based rare-earth free external rotor PMa-SynRMs have

performed better under SE conditions, however, rare-earth based designs have lower torque pulsations at higher eccentricity conditions. In conclusion, rare-earth free based PMa-SynRMs can be considered as equally competitive to rare-earth based PMa-SynRM under SE, DE, and ME fault conditions. Also, with respect to back-EMF, rare-earth free based PMa-SynRM has higher 3rd harmonics compared to the rare-earth based PMa-SynRM.

VIII. REFERENCES

[1] B. M. Ebrahimi, M. Javan Roshtkhari, J. Faiz and S. V. Khatami, "Advanced Eccentricity Fault Recognition in Permanent Magnet Synchronous Motors Using Stator Current Signature Analysis," in *IEEE Transactions on Industrial Electronics*, vol. 61, no. 4, pp. 2041-2052, April 2014.

[2] J. Hong *et al*., "Detection and Classification of Rotor Demagnetization and Eccentricity Faults for PM Synchronous Motors," in *IEEE Transactions on Industry Applications*, vol. 48, no. 3, pp. 923-932, May-June 2012.

[3] K. Kang, J. Song, C. Kang, S. Sung, G. Jang, "Real-time Detection of the Dynamic Eccentricity in Permanent Magnet Synchronous Motors by Monitoring Speed and Back EMF Induced in an Additional Winding," in *IEEE Transactions on Industrial Electronics*, vol.64, no.9, pp.7191-7200, 2017.

[4] J. Faiz and M. R. Hassan-Zadeh, "Impacts of eccentricity fault on permanent magnet generators for distributed generation," *2017 International Conference on Optimization of Electrical and Electronic Equipment (OPTIM) & 2017 Intl Aegean Conference on Electrical Machines and Power Electronics (ACEMP)*, Brasov, 2017, pp. 434-441.

[5] E. Pazouki, M. Z. Islam, S. S. R. Bonthu and S. Choi, "Eccentricity fault detection in multiphase permanent magnet assisted synchronous reluctance motor," *2015 IEEE International Electric Machines & Drives Conference (IEMDC)*, Coeur d'Alene, ID, 2015, pp. 240-246.

[6] S. M. Mirimani, A. Vahedi, F. Marignetti and R. Di Stefano, "An Online Method for Static Eccentricity Fault Detection in Axial Flux Machines," in *IEEE Transactions on Industrial Electronics*, vol. 62, no. 3, pp. 1931-1942, March 2015.

[7] L. J. Wu, Z. Q. Zhu, Y. T. Fang and X. Y. Huang, "Difference in unbalanced magnetic force of fractional-slot PM machines between internal and external rotor topologies," in *CES Transactions on Electrical Machines and Systems*, vol. 1, no. 2, pp. 154-163, 2017.

[8] S. S. R. Bonthu, S. Choi and J. Baek, "Design Optimization with Multi-physics Analysis on External Rotor Permanent Magnet Assisted Synchronous Reluctance Motors," in *IEEE Transactions on Energy Conversion*, vol. PP, no. 99, pp. 1-1.

[9] S. S. R. Bonthu, A. Arafat and S. Choi, "Comparisons of Rare-Earth and Rare-Earth-Free External Rotor Permanent Magnet Assisted Synchronous Reluctance Motors," in *IEEE Transactions on Industrial Electronics*, vol. 64, no. 12, pp. 9729-9738, Dec. 2017.

[10] S. S. R. Bonthu and S. Choi, "Design procedure for multi-phase external rotor permanent magnet assisted synchronous reluctance machines," *2016 IEEE Applied Power Electronics Conference and Exposition (APEC)*, Long Beach, CA, 2016, pp. 1131-1137.

[11] S. Bonthu, S. Choi, A. Gorgani and K. Jang, "Design of permanent magnet assisted synchronous reluctance motor with external rotor architecture," in *IEEE International Electric Machines & Drives Conference (IEMDC)*, Coeur d'Alene, 2015.

[12] S. Choi and S. S. R. Bonthu, "Method for design and customization of a multiphase electric motor," U.S. Patent 14/825,834, Feb. 18, 2016.

[13] Y. Li, Q. Lu and Z. Q. Zhu, "Unbalanced magnetic force prediction in permanent magnet machines with rotor eccentricity by improved superposition method," in *IET Electric Power Applications*, vol. 11, no. 6, pp. 1095-1104, 7 2017.

[14] S. S. R. Bonthu, M. Z. Islam, A. Arafat and S. Choi, "Five-phase external rotor permanent magnet assisted synchronous reluctance motor for in-wheel applications," *2017 IEEE Transportation Electrification Conference and Expo (ITEC)*, Chicago, IL, 2017, pp. 586-591.

[15] S. S. R. Bonthu, M. Z. Islam and S. Choi, "Design of a rare earth free external rotor permanent magnet assisted synchornous reluctance motor," *2017 IEEE International Electric Machines and Drives Conference (IEMDC)*, Miami, FL, 2017, pp. 1-6.